Role of Hydrodynamic Drag on Microsphere Deposition and Re-entrainment in Porous Media under Unfavorable Conditions

X I Q I N G L I , [†] P E N G F E I Z H A N G , [†,‡]
C . L . L I N , [§] A N D W I L L I A M P . J O H N S O N * , [†]

Department of Geology and Geophysics and Department of Metallurgical Engineering, University of Utah, Salt Lake City, Utah 84112

Deposition and re-entrainment of 1.1 μm microspheres were examined in packed glass beads and quartz sand under both favorable and unfavorable conditions for deposition. Experiments were performed at environmentally relevant ionic strengths and flow rates in the absence of solution chemistry and flow perturbations. Numerical simulations of experimental data were performed using kinetic rate coefficients to represent deposition and re-entrainment dynamics. Deposition rate coefficients increased with increasing flow rate under favorable deposition conditions (in the absence of colloid-grain surface electrostatic repulsion), consistent with expected trends from filtration theory. In contrast, under unfavorable deposition conditions (where significant colloid-grain surface electrostatic repulsion exists), the deposition rate coefficients decreased with increasing flow rate, suggesting a mitigating effect of hydrodynamic drag on deposition. Furthermore, the re-entrainment rate was negligible under favorable conditions but was significant under unfavorable conditions and increased with increasing flow rate, demonstrating that hydrodynamic drag drove re-entrainment under unfavorable conditions. The drag torque resulting from hydrodynamic drag was found to be 1 order of magnitude or more lower than the adhesive torque based on pull-off forces from atomic force microscopy measurements. This result indicates that hydrodynamic drag was insufficient to drive re-entrainment of microspheres that were associated with the grain surface via the primary energy minimum and suggests that hydrodynamic drag drove re-entrainment of secondary-minimum-associated microspheres.

Introduction

Deposition and re-entrainment dynamics of colloids (e.g. minerals and microbes less than 10 μm in diameter) govern their distance and rate of transport in porous media and so are important to drinking water treatment and protection. Colloid re-entrainment occurs ubiquitously in the absence of macroscopic perturbations in solution chemistry and flow (*1−19*) and may serve to translate retained colloids downgradient at significant rates in some systems (*17*). In most

environmental systems, where both colloids and sediments typically carry overall negative surface charge (*20, 21*), an energy barrier to colloid deposition exists, and this condition is considered "unfavorable" for colloid deposition. However, colloid deposition occurs despite the presence of apparently large energy barriers (e.g. 100s of kT). Multiple mechanisms, such as surface charge heterogeneity and roughness (*22, 23*), may effectively eliminate energy barriers, thereby creating locally favorable deposition conditions.

Colloid re-entrainment investigations (*24−28*) have mostly focused on the effects of perturbations in flow and solution chemistry on colloid re-entrainment. In these studies, it is a common practice to deposit the colloids onto the surface under favorable conditions, where retained colloids would be expected to be directly associated with the collector surfaces via the primary energy minima. Under these conditions, colloid re-entrainment is thought to be initiated by rolling on the collector surface (*25*), since hydrodynamic lift is insufficient relative to the adhesive force to drive re-entrainment (*27*). Initiation of rolling requires dominance of the drag torque relative to the adhesive torque (*28*), which can be brought about by perturbations in solution chemistry and flow condition. In contrast, the factors governing re-entrainment in the absence of macroscopic perturbations (constant solution chemistry and flow rate) have not been well investigated or understood.

Colloid deposition rate coefficients have been shown to decrease with increasing flow rate (*29−31*) under unfavorable deposition conditions, leading to the suggestion that these trends represent effects of hydrodynamic drag. However, these suggestions need to be placed on a firmer basis by comparison to colloid deposition theory and comparison to deposition under favorable conditions. Furthermore, the mechanism(s) by which hydrodynamic drag would cause the observed trends in deposition rate coefficient versus flow rate need to be elucidated.

The purpose of this paper is to examine the trends versus ionic strength and flow rate in the kinetic parameters describing the dynamics of colloid deposition and re-entrainment in the absence of macroscopic perturbations. It was found that deposition rates increased with increasing flow rate under favorable conditions in agreement with theory, whereas the opposite trend was observed under unfavorable conditions. Furthermore, the re-entrainment rate under unfavorable conditions increased strongly with flow rate, whereas re-entrainment was negligible under favorable deposition conditions. These results suggest a change in the nature of deposition between favorable and unfavorable conditions such that colloids deposited under unfavorable deposition conditions were relatively vulnerable to hydrodynamic drag. The mechanisms by which hydrodynamic drag mitigates deposition and drives re-entrainment under unfavorable conditions are examined in the context of particle deposition models, as well as by comparison of the torques driving and resisting re-entrainment

Methods

Experimental. The colloids used in the porous media transport experiments under unfavorable deposition conditions were spherical fluorescent carboxylate-modified polystyrene latex microspheres with a diameter of 1.1 μm. The microsphere stock suspensions (Molecular Probes, Inc., Eugene, OR) were used as received with a particle concentration of 2.7×10^{10} partilce mL^{-1}. Prior to injection, an aliquot of stock suspension was diluted to achieve an influent concentration (C_o) of $3.5 \times 10^6 \pm 15\%$ particles mL^{-1} in salt

---

* Corresponding author phone: 801-581-5033; fax: 801-581-7065; e-mail: wjohnson@mines.utah.edu.
† Department of Geology & Geophysics.
‡ Present address: Department of Earth and Atmospheric Sciences, City College of New York, CUNY, New York City, NY.
§ Department of Metallurgical Engineering.

solutions with desired ionic strengths. Positively charged amine-modified polystyrene latex microspheres (diameter = 0.93 μm) (Molecular Probes, Inc., Eugene, OR) were used in experiments examining favorable deposition conditions. The stock suspension (4.5×10^{10} particles mL^{-1}) of the amine-modified microspheres was diluted to achieve an influent concentration of 1.5×10^7 particles mL^{-1}.

The porous media used in the column experiments was 30−40 mesh (417−600 μm) soda lime glass beads (Cataphote Inc., Jackson, MS) and quartz sand (Unimin Corp., New Canaan, CT). The glass beads were first rinsed sequentially with acetone and hexane and then soaked with concentrated HCl for about 24 h, followed by repeated rinsing with ultrapure water (Millipore Corp. Bedford, MA) until the ionic strength was negligible relative to the experimental ionic strength. The quartz sand was cleaned by soaking in concentrated HCl for at least 24 h, followed by repeated rinsing with ultrapure water (Millipore Corp. Bedford, MA), drying at 105 °C, and baking overnight at 850 °C. Prior to the column experiments, the sand was rehydrated by boiling in pure water for at least 1 h.

Cylindrical plexiglass columns (20 cm in length and 3.81 cm in inner diameter) were dry-packed after the cleaned glass beads and rehydrated quartz sand were dried at 105 °C and cooled. The porosity of the packed glass beads and quartz sand were 0.37 and 0.36, respectively. The columns packed with glass beads were purged with CO_2 for at least 15 min and were then flushed with HCl solution at pH 3.0 for 24 h at an average flow rate of 2.8 mL min^{-1}. This flushing with pH 3.0 solution was intended to dissolve Na_2O and CaO at the glass bead surface and allow subsequent pH equilibration (32). After flushing, the columns were pre-equilibrated overnight (at a flow rate of 0.6 mL-min^{-1}) for about 10 pore volumes with microsphere-free salt solution at pH of 6.92, buffered by MOPS/NaOH. Following pre-equilibration, the effluent pH consistently differed by no more than 0.02 units from that of the influent. The columns packed with quartz sand were pre-equilibrated immediately after CO_2 purging with the same pore volumes of solutions at same pH, using the same buffer.

After pre-equilibration, 3 pore volumes of microsphere suspension was injected, followed by elution with 7 pore volumes of buffered salt solution (without microspheres) at the same ionic strength and pH. The suspensions and solutions were injected in up-flow mode using a syringe pump (Harvard Apparatus Inc., Holliston, MA). During injection, the microsphere suspension reservoirs were sonicated for 1 min each hour to minimize aggregation. The transport experiments with the carboxylate-modified microspheres were carried out at three ionic strengths, 0.006, 0.02 and 0.05 M, in glass beads and at four ionic strengths, 0.001, 0.003, 0.006 and 0.02 M, in quartz sand. The flow rate was varied to produce pore water velocities of 2, 4, and 8 m day^{-1}. The transport experiments with the amine-modified microspheres in both porous media were carried out at 0.001 M ionic strength and at flow rates of 4 and 8 m day^{-1}.

Column effluent samples were collected in 5-mL polystyrene tubes with a fraction collector (CF-1, Spectrum Chromatography, Houston, TX). Following the experiment, the sediment was dissected into 10 2-cm-long segments, as the sediment was released from the column under gravity. Retained colloids were recovered by placing sediment segments (2 cm) into specified volumes of Milli-Q water and sonicating for 1 min, followed by manual vigorous shaking for a few seconds. These specified volumes were 100 mL for the first three segments at the column inlet and 25 mL for all subsequent segments. Aqueous effluent samples and supernatant samples from recovery of retained microspheres were analyzed using flow cytometry (BD FACScan, Becton Dickinson & Co., Franklin Lakes, NJ). Additional details of

the column experiment procedure, sample collection, and analysis were provided in two previous papers (33, 34).

Modeling. The transport of the microspheres was modeled using an advection−dispersion equation that includes deposition from, and re-entrainment to, the aqueous phase:

$$\frac{\partial C}{\partial t} = -v\frac{\partial C}{\partial x} + D\frac{\partial^2 C}{\partial x^2} - k_f C + \frac{\rho_b}{\theta}k_r S_r \tag{1}$$

where C is the microsphere concentration in the aqueous phase (particles per unit volume of fluid), t is the travel time, x is the travel distance, v is the flow velocity, D is the dispersion coefficient of the colloid particles, θ is the porosity, ρ is the bulk density of sediment, and k_f and k_r are rate coefficients of microsphere deposition to and re-entrainment from solid phase, respectively. S_r is the reversibly retained microsphere concentration on the solid phase (particles per unit mass of sediment) and can be further expressed as

$$S_r = S(1 - f_{ir}) \tag{2}$$

where S is the total removed concentration and f_{ir} is the fraction of reversibly deposited colloids. In this work, the reversibility of deposition is expressed as fraction of reversibly deposited colloids, f_r ($= 1 - f_{ir}$). A one-dimensional discrete random-walk particle-tracking model was used to simulate microsphere transport (eqs 1 and 2). The representation of k_f, k_r, and f_{ir} in the particle model is described in detail elsewhere (17, 33, 35). It is important to note that the probabilistic approach used in the particle tracking model decouples the parameters k_r and f_{ir}, whereas this decoupling is not apparent in the equations as written in continuum form (eqs 1 and 2).

Magnitudes and trends of the deposition rate coefficients can be compared with expectations from theory based on following equation

$$k_f = \frac{3}{2}\frac{(1 - \theta)}{d_c}v\alpha\eta \tag{3}$$

where d_c is the grain diameter and α is the collision efficiency, which is treated as constant for a given ionic strength. The single collector efficiency, η, can be calculated using the correlation equations developed by Rajagopalan and Tien (36, 37) and by Tufenkji and Elimelech (38), abbreviated below as the R−T and T−E equations, respectively.

Torque Evaluation. The drag torque (T_D) experienced by a retained colloid at the grain surface due to the drag force (F_D), is expressed as (27, 39−41)

$$T_D = 1.399 a_{colloid} F_D \tag{4}$$

where $a_{colloid}$ is the retained colloid radius and the leading coefficient (1.399) indicates that the drag force acts effectively on the deposited colloid at a distance of 1.399 $a_{colloid}$ from the surface. The drag force is related to the fluid velocity at the center of the retained colloid, the colloid radius, and the fluid viscosity (μ) (39−41)

$$F_D = (1.7005)6\pi\mu v_{colloid} a_{colloid} \tag{5}$$

where the leading coefficient (1.7005) accounts for the wall effects near the grain surface.

The fluid velocity at the center point of the retained colloid can be derived from a representative pore structure using the constricted tube model (28, 42), in which the pore space is comprised of a series of parabolic constrictions, the diameter (d_z) of which is a function of distance along the pore (z)

$$d_z = 2\left\{\frac{d_{max}}{2} + \left[4\left(\frac{d_c}{2} - \frac{d_{max}}{2}\right)\left(0.5 - \frac{z}{h}\right)^2\right]\right\} \tag{6}$$

where d_c is the equivalent diameter of the constriction, d_{max} is the maximum pore diameter, and h is the pore length. The fluid velocity at the center point of the retained colloid can be determined as follows (28)

$$v_{colloid} = \frac{Q/N_{pore}}{(\pi/4)d_z^2} \frac{4(d_z/2 - a_{colloid})}{(d_z/2)^2} \quad (7)$$

where Q is the volumetric flow rate in the porous media and N_{pore} is the number of pores in the column cross section. The irregular shape of the quartz sand grains prevented the application of the constricted tube model to this media. Therefore, the torque analysis was restricted to glass beads.

Preliminary work was also conducted to characterize the pore structure within a specimen of 40−50 mesh glass beads media (4 × 4 × 3.12 mm) using cone-beam X-ray microtomography (XMT) with a reconstruction resolution of 20 μm. Fluid flow in the pore domain was simulated using a Lattice−Boltzmann (LB) model that yielded discreet flow velocities at 20 μm resolution. Detailed descriptions of the XMT scanning protocol and the LB simulations are provided in Lin and Miller (43, 44). The velocities obtained from this approach represented values at distances within 20 μm from the grain surfaces. To allow interpolation of velocities at the center point of the retained colloids (about 0.55 μm from the surface), hydrodynamic shear within 20 μm of the grain surface was approximated by subtracting velocities at the grain surface (zero) from the closest lattice point velocity and dividing by 20 μm. The distribution of hydrodynamic shear was multiplied by 0.55 μm to yield the velocities at a distance of 0.55 μm from the surface.

The adhesive torque (T_A) is represented by the adhesion force (F_A) acting on a lever arm l_x:

$$T_A = F_A l_x \quad (8)$$

The lever arm is provided by the radius of colloid-surface contact (a_0), which results from deformation of the microsphere (41, 45−47) or deformation of the grain surface. In our system, deformation of the grain surface is expected to be negligible compared to that of the microsphere, since the Young's modulus of elasticity of glass, 6.9 × 10^{10} N m^{−2}, is much greater than that of polystyrene, 0.28 × 10^{10} N m^{−2} (46). Therefore, the microsphere will deform to yield a contact radius that is proportional to the adhesion force (48)

$$a_0 = (4F_A a_{colloid}/K)^{1/3} \quad (9)$$

where K is the elastic interaction constant, 4.0 × 10^9 N m^{−2} (46).

The adhesion force was approximated by the pull-off force measured using atomic force microscopy (AFM) between a glass surface and the microspheres. The microspheres used for force measurement were from a different batch (with the same catalog number from the same manufacturer) than the one used for column experiments. The microspheres used in AFM measurements displayed greater negative ζ-potential than the microspheres used for column experiments (e.g., −98.4 vs −63.2 mV at 0.02 M). The microspheres were glued to the tip of rectangular cantilevers (Mikromash, Burgdorf, Switzerland) using a micromanipulator, and the glue (Norland Optical Adhesive 63, Norland Products, Cranbury, NJ) was UV-cured for 2 min. The spring constant of the cantilever was determined as 0.06 N m^{−1} using the Sader method (49). An MFP3D atomic force microscope (Asylum Research, Santa Barbara, CA) at the University of Geneva was used for AFM force measurements with a scan size of 1.07 μm and a scan rate of 0.15 Hz. Measurements were made in solution (200-μL droplet on the glass slide). Time of measurement was limited (e.g., 15−30 min) to avoid

significant concentration of electrolyte by evaporation. The raw data (voltage versus deflection) was converted to force versus distance using Asylum Research MFP3D software.

DLVO Interaction Energy Profiles. To support interpretation of trends in deposition rate coefficients, the interaction energies as a function of separation distance between the 1.1-μm microsphere and the glass beads were calculated using DLVO theory. The electrophoretic mobilities of the microspheres, crushed glass beads, and crushed quartz sand were measured using a ZetaPALS Analyzer (Brookhaven Instruments, Holtsville, NY) and were converted to ζ-potentials using the von Smoluchowski approach. The ζ-potentials for the microspheres were −65.3, −63.2, and −51.78 mV for the 0.006, 0.02, 0.05 M ionic strengths, respectively. The ζ-potentials of the crushed glass beads were −67.5, −64.0, and −57.0 mV for the 0.006, 0.02, 0.05 M ionic strengths, respectively. The ζ-potentials of crushed quartz sand were very similar to those of the crushed glass beads. The electrostatic repulsive interaction and retarded van der Waals attractive interaction were calculated on the basis of approximate expressions developed by Gregory (50, 51). The decay length for the van der Waals interaction was 100 nm and the Hamaker constants were 3.8 × 10^{−21} and 6.8 × 10^{−21} J for the microsphere−water−glass system (52) and the microsphere−water−quartz system (34), respectively.

Results

Transport in Porous Media. Deposition of carboxylate-modified microspheres (unfavorable deposition conditions) increased with increasing ionic strength and decreased with increasing flow, as shown by the magnitudes of the breakthrough plateaus (Figures 1 and 2, parts A and B) and the profiles of retained microspheres (Figures 1 and 2, parts C and D). The amine-modified microspheres showed greater deposition (favorable deposition conditions) relative to the carboxylate-modified microspheres (unfavorable deposition conditions), as expected (Figures 1 and 2). Error bars represent standard deviations from replicate experiments ($n \geq 2$). Mass recoveries (total from effluent and sediment) were very good, virtually all between 86% and 107%, with the vast majority showing between 95% and 105% recovery (33, 34). Under a few experimental conditions (0.02 M and 2 m day^{−1} in glass beads; 0.02 M and 4 m day^{−1} in quartz sand; and 0.006 M and 2 m day^{−1} in quartz sand), declining breakthrough concentrations during injection (slight under the latter two conditions) were observed, indicating the occurrence of ripening, a process resulting from deposited colloids acting as additional deposition sites. These experimental conditions were simulated with a temporally constant deposition rate coefficient that reflected the average deposition rate coefficient during the experiment.

The magnitude of the eluted concentrations showed no clear trend with ionic strength and flow rate (Figures 1 and 2, parts A and B), since re-entrainment rates are a function of retained concentrations as well as solution conditions. Hence, re-entrainment rate coefficients could not be discerned directly from the eluted concentrations, requiring their determination via kinetic modeling. Comparison to transport of a conservative tracer (tritiated water) demonstrated that the extended tailing of low concentrations of colloids during elution was driven by re-entrainment and not by the potential presence of nonadvective pore space (data not shown).

Under favorable deposition conditions, the concentrations of retained amine-modified microspheres in glass beads and quartz sand (favorable deposition conditions) decreased with distance from the column inlet log-linearly (Figures 1 and 2, parts C and D), as expected from filtration theory, which assumes a spatially constant deposition rate coefficient, k_f. In contrast, the profiles of retained carboxylate-modified
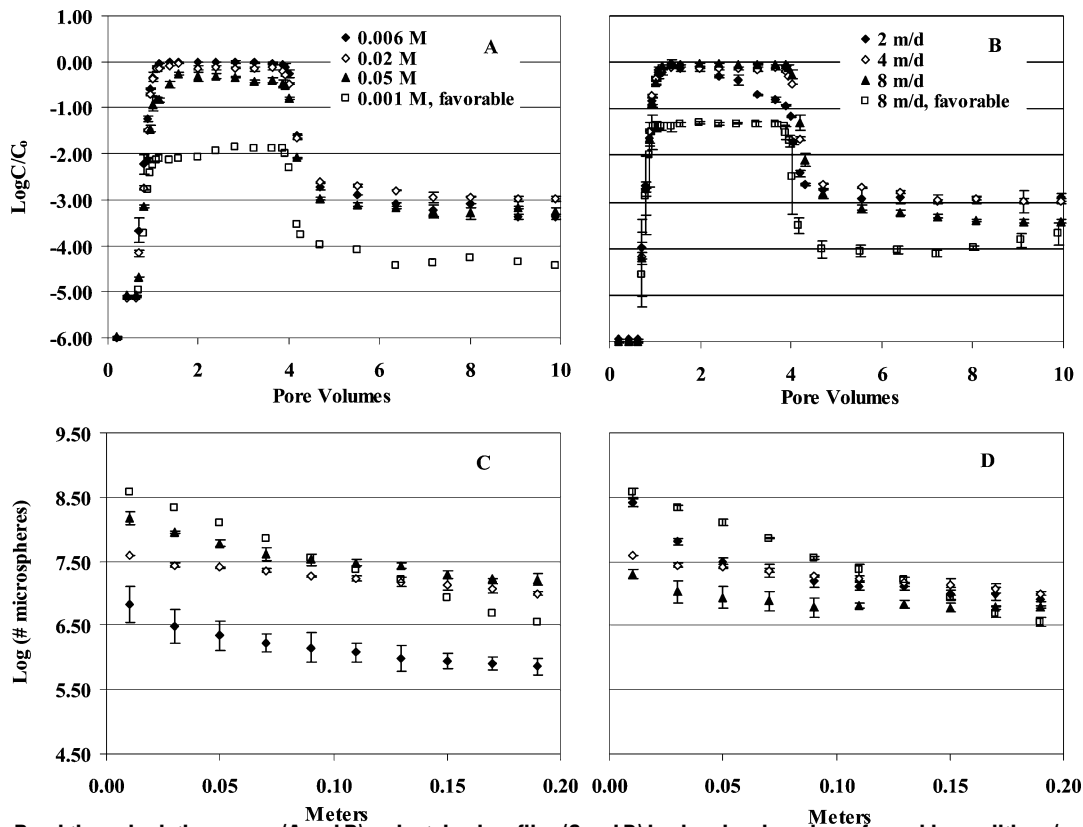
FIGURE 1. Breakthrough-elution curves (A and B) and retained profiles (C and D) in glass beads under unfavorable conditions (carboxylate-modified microspheres) and favorable conditions (amine-modified microspheres). Ionic strength series (4 m day^{-1}) is shown on left. Flow rate series (0.02 M for unfavorable, 0.001 M for favorable) is shown on right. Error bars represent standard deviations in results from replicate experiments ($n \geq 2$). The influent concentration of amine-modified microspheres (1.5 × 10^7 particles mL^{-1}) was normalized to the average influent concentration of carboxylate-modified microspheres (3.5 × 10^6 particles mL^{-1}).
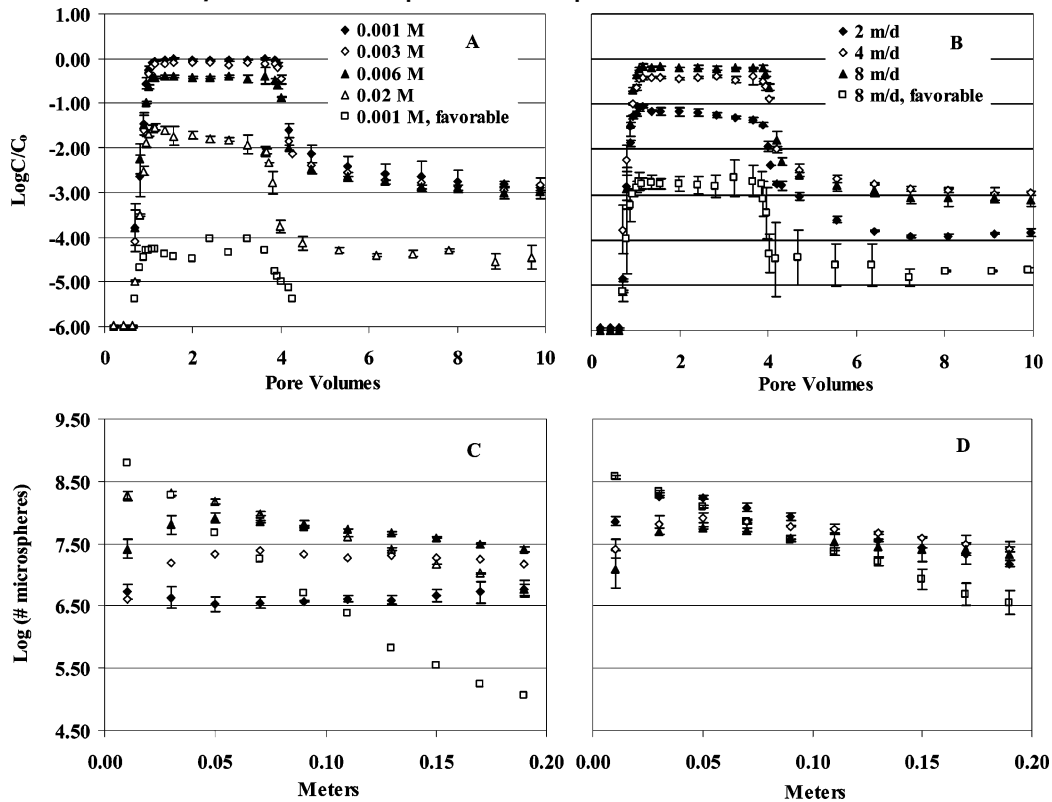

FIGURE 2. Breakthrough-elution curves (A and B) and retained profiles (C and D) in quartz sand under unfavorable conditions (carboxylate-modified microspheres) and favorable conditions (amine-modified microspheres). Ionic strength series (4 m day^{-1}) is shown on left. Flow rate series (0.006 M for unfavorable, 0.001 M for favorable) is shown on right Error bars represent standard deviations in results from replicate experiments ($n \geq 2$). The influent concentration of amine-modified microspheres (1.5 × 10^7 particles mL^{-1}) was normalized to the average influent concentration of carboxylate-modified microspheres (3.5 × 10^7 particles mL^{-1}).
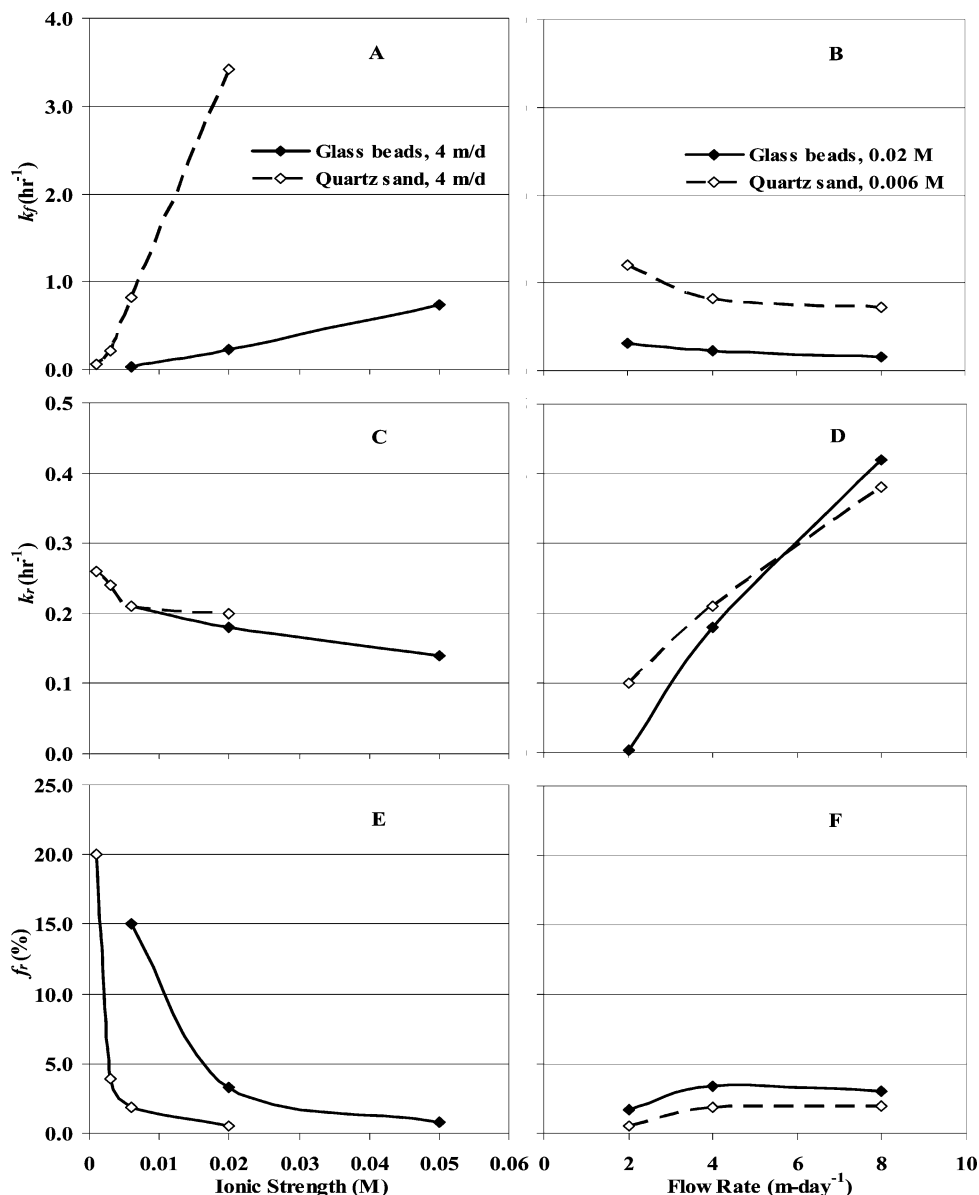
FIGURE 3. Deposition rate coefficient (k_f, A and B), re-entrainment rate coefficient (k_r, C and D), and fraction of reversible deposition (f_r, E and F) for the ionic strength series (4 m day^{-1}) and the flow rate series (0.02 M for glass beads, 0.006 M in quartz sand).

microspheres in glass beads and quartz sand (unfavorable deposition conditions) deviated from log-linearity (Figures 1 and 2, parts C and D). The form and extent of deviation from log-linear behavior were quantified using a particle-tracking model with a log-normal distribution of deposition rate coefficients, as described in a previous publication (*33*).

Kinetic Parameters. Analysis of the trends in the deposition and re-entrainment rate coefficients versus ionic strength and flow rate was simplified in this paper by the use of the particle-tracking model with a single spatially invariant deposition rate coefficient. Although the spatially invariant deposition rate coefficient model could not simulate the shapes of the retained microsphere profiles, it produced equivalent parameter trends relative to the distributed deposition rate coefficient model (*33*).

The trends in kinetic parameters versus ionic strength and flow rate were highly consistent between the two porous media (glass beads and quartz sand) (Figure 3), indicating that the observed trends were not specific to particular shapes of sediment grains (spherical glass beads versus angular quartz sand). However, the magnitudes of the deposition rate coefficients were much greater in the quartz sand relative

to the glass beads, indicating enhancement of deposition rate coefficients by surface roughness or angularity associated with the quartz sand.

The deposition rate coefficient (k_f) increased dramatically with increased ionic strength (Figure 3A), as has been demonstrated in numerous other studies, consistent with compression of the electrostatic double layer surrounding the surfaces. The fraction of reversibly deposited microspheres (f_r) was extremely low under favorable deposition conditions (0.4% and 0.8% in glass beads, 0 and 1.2% in quartz sand, at 4 and 8 m day^{-1}, respectively) relative to unfavorable deposition conditions at the same flow rates (Figure 3F). The fraction of reversible deposition decreased greatly with increased ionic strength (Figure 3E).

The magnitudes of the observed deposition rate coefficients (k_f) under favorable deposition conditions ($\alpha = 1$) qualitatively agreed with values predicted using eq 3 and the correlation equations (R–T and T–E equations) for the collector efficiency (Figure 4), especially those for the glass beads. Deposition rate coefficients increased with increasing flow rate for both theoretical and observed values under favorable conditions in both porous media. In contrast,
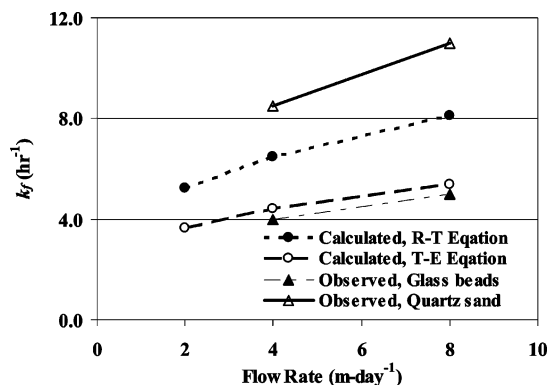
FIGURE 4. Theoretical and experimental deposition rate coefficients under favorable deposition conditions (positively charged amine-modified polystyrene microspheres). Theoretical deposition rate coefficients were calculated as described in the Methods section.
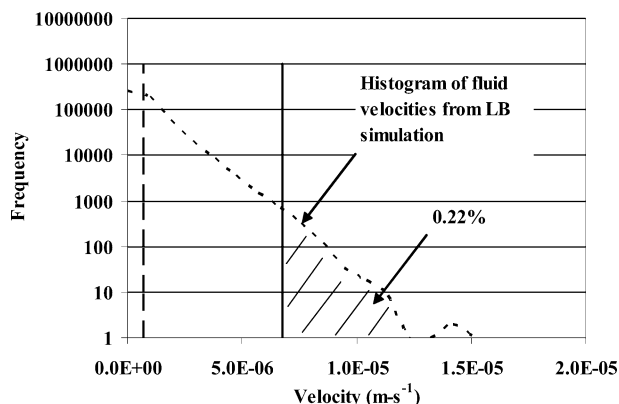

FIGURE 5. XMT-LB velocities at 0.55 μm distance from the grain surface in 40−50 mesh glass beads (4 m day^{-1}, dashed curve) and constricted tube model velocities at the same separation distance and flow rate (vertical lines represent minimum and maximum velocities at the pore opening and the pore constriction, respectively).

FIGURE 6. Calculated DLVO interaction energy between the 1.1-μm carboxylated microsphere and glass bead surface as a function of separation distance. The secondary minima are shown in the insert. The interaction energy was calculated from experimentally measured ζ-potentials and with a Hamaker constant of 3.8×10^{-21} J.

deposition rate coefficients under unfavorable conditions decreased with increasing flow rate (Figure 3B).

Re-entrainment rates under unfavorable deposition conditions increased directly with increasing flow rate, with about a factor of 2 or more increase in k_r correspondent with a factor of 2 increase in flow rate (Figure 3D). In contrast, the eluted concentrations (k_r) were relatively negligible (at 8 m day^{-1} in quartz sand) under favorable deposition conditions.

Torque Comparison. The magnitudes of the center point velocities at 0.55 μm from the surface in 40−50 mesh glass beads are shown in Figure 5. Only about 0.2% of the center point velocities determined using XMT-LB were greater than the maximum velocities obtained from the constricted tube model. The maximum velocity from XMT-LB was only a factor of 2.5 greater than that from the constricted tube model. Hence, the constricted tube model appears to have reasonably captured the bulk characteristics of the flow field adjacent to the grain surfaces. The maximum drag torque in the 30−40 mesh glass beads based on the constricted tube model was 1.27×10^{-19} N m, yielding an estimated maximum drag torque of 3.2×10^{-19} N m in the XMT-determined pore domain. This estimate assumed that the ratio of the maximum velocities between the XMT-LB and constricted tube approaches (2.5) determined for the 40−50 mesh glass beads also applied to the 30−40 mesh glass beads.

The minimum adhesion force measured by AFM in a system with polystyrene latex microspheres similar to those used in the column experiments (see Methods) was found to be 5.7×10^{-10} N under ionic strength conditions equivalent
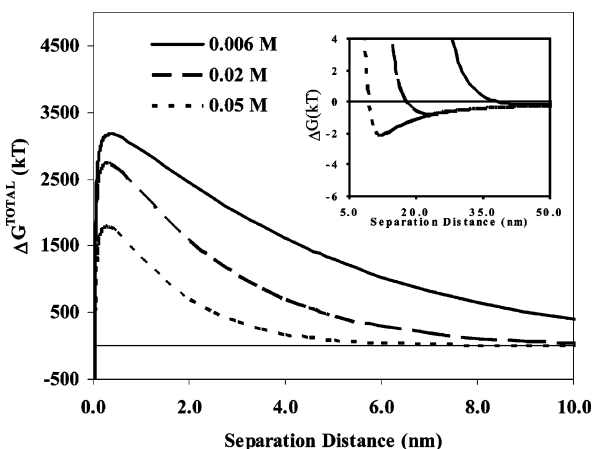
to the column experiments. The corresponding contact radius estimated using eq 9 was 6.8 nm. If the glass bead surface were perfectly smooth (lacking surface asperities), this contact radius might serve as the lever arm defining the adhesive torque (41), assuming rolling is initiated by "tipping" the microsphere off the contact radius. However, the glass bead surfaces showed asperities against which the microspheres might rest, thereby enhancing the adhesive torque (41). Trigonometry indicates that even a 0.5-nm-high protrusion can provide an effective lever arm of 23.5 nm, a value that is much greater than the 6.8-nm lever arm based on microsphere deformation on a flat surface (eq 9). Alternatively, if the microspheres rested atop closely spaced surface asperities, the actual contact area would be decreased relative to that expected from eq 9 (53). Measured root-mean-square surface roughness of the glass beads was 15.0 ± 1.9 nm, with distances between asperities being much greater than the size of the 1.1-μm microspheres (22), indicating that the retained microspheres should reside between asperities, rather than atop multiple asperities. The adhesive torque is therefore expected to be enhanced by the surface asperities, and the adhesive torque corresponding to the 6.8-nm lever arm is considered to represent a lower bound estimate of the actual adhesive torques. This lower bound adhesive torque was 3.9×10^{-18} N m, a value 30 or 12 times greater than the maximum drag torques (1.27×10^{-19} and 3.2×10^{-19} N m) from the constricted tube and XMT-LB approaches, respectively.

Discussion

The deposition rate coefficient (k_f) increased with increasing ionic strength (Figure 3A), as expected from DLVO considerations. The kinetic model provides the further unique observation that the fraction of reversibly retained colloids (f_r) decreased with increasing ionic strength (Figure 3E). The trend in f_r demonstrates that, as ionic strength increased, an increasingly larger fraction of the microspheres were "deposited" in energy minima that were sufficiently deep to prevent re-entrainment. That the minima of the calculated interaction energies between the carboxylate-modified microspheres and the porous media (glass beads) grain surfaces deepened with increasing ionic strength is demonstrated in Figure 6.

The observed trends in deposition and re-entrainment coefficients versus flow rate suggest that deposition under unfavorable conditions yields increased vulnerability of

deposited colloids to hydrodynamic drag. Under favorable deposition conditions, the deposition rate coefficient increased with increasing flow rate (Figure 4), in agreement with theory (T−E and R−T correlation equations), and re-entrainment rates were negligible. In contrast, under unfavorable deposition conditions, the deposition rate coefficients decreased, and the re-entrainment rate coefficients increased, with increasing flow rate. These differences signal an important change in the nature of deposition under unfavorable relative to favorable conditions. This change in deposition mechanism is also demonstrated by the profile of retained colloids, which decreased log-linearly from the source under favorable conditions, but which deviated from log-linearity under unfavorable conditions (33, 34, 54).

Vulnerability of deposited colloids to hydrodynamic drag depends on the mechanism of deposition. Colloid deposition to grain surfaces has traditionally been considered to occur via the primary energy minimum, which is considered a "perfect sink" boundary at which the colloid is effectively removed from solution (55) and is no longer subject to a hydrodynamic force. More recently, deposition in the secondary energy minimum has been promoted as an important mechanism of deposition under unfavorable conditions (56), on the basis that significant fractions of deposited colloids are released upon elution with pure water (54, 56, 57), which eliminates secondary energy minima but preserves primary energy minima.

Hydrodynamic drag may indirectly decrease colloid deposition "within" the primary energy minimum by decreasing the particle flux over the energy barrier under conditions where a low energy barrier (<15 kT) and a deep secondary minimum (>5 kT) exist (58, 59). Under these interaction energy conditions, colloid accumulation within the secondary energy minimum occurs and indirectly mitigates deposition in the primary minimum (decreases colloid flux to the primary minimum), due to tangential flux of secondary-minimum-associated colloids in response to tangential hydrodynamic drag (58, 59). This effect of tangential flux of secondary-minimum-associated colloids was demonstrated via particle transport models in simple shear systems for Peclet numbers between about 0.001 and about 20 (58, 59). This effect could potentially explain decreases in k_f with increasing flow rate for colloids deposited "within" primary minima, i.e., in an impinging jet system, where secondary-minimum colloids are swept from the observation area by hydrodynamic drag (60). The experiments in the impinging jet system (60) and the experiments described here in porous media were performed at equivalent Peclet numbers (based on tangential velocities one colloid radius from the surface) ranging from 0.5 to 30. By extension, tangential colloid flux may potentially explain the decrease in k_f with increasing flow rate shown here for colloid transport in porous media. Although the interaction energy profiles calculated here displayed significant energy barriers (>1500 kT) and shallow secondary energy minima (<2.5 kT) (Figure 6), these values were based on bulk measured properties and so may not represent the actual interaction energy conditions, which can be expected to show a distribution due to surface nonidealities (e.g. heterogeneity in charge and roughness).

The observed trend of increasing re-entrainment rates with increasing flow rate demonstrates that hydrodynamic drag directly influenced re-entrainment and, by extension, deposition. The mechanisms of re-entrainment differ depending on the environment of deposition. Re-entrainment of colloids deposited "within" a primary minimum requires that the drag torque rival the adhesive torque for attached colloids. The maximum hydrodynamic torque was lower than the AFM-based adhesive torque by over 1 order of magnitude (described above), which seems to preclude the possibility

of re-entrainment of colloids from the primary minimum. However, as mentioned above, a distribution of adhesive torques likely exists due to surface nonidealities, possibly allowing re-entrainment of a portion of the population of primary-minimum associated microspheres. The adhesive force that would yield an adhesive torque equal to the maximum drag torque (3.2×10^{-19} N m) can be determined using eqs 8 and 9. A primary energy minimum of 3.4 kT or less would be required to yield a sufficiently low adhesive force, based on the Derjaguin and Langbein approximations (48, 28), assuming a closest separation distance of 0.158 nm (28). This diminutive depth for the primary energy minimum is far smaller than would be reasonably expected, indicating that tangential hydrodynamic drag is insufficient to drive re-entrainment of primary-minimum-associated colloids. Although the above considerations do not eliminate the possibility of re-entrainment from the primary minimum in this system, they do argue effectively against it.

The above analysis points toward re-entrainment of colloids from the secondary minimum in this system. Association of colloids with the secondary energy minimum should result in tangential flux of colloids across the porous media grain surfaces until they reach features that would locally halt the tangential flux, e.g., zones of stagnation flow created by grain surface asperities or rear stagnation points, as well as asperities that may act as lever arms to create adhesive torques that halt tangential movement (20, 24, 25). Experiments using the same microspheres, solution conditions, and surface velocities as examined here were performed on quartz and glass substrata in an impinging jet system (60) in order to compare colloid deposition in systems lacking (impinging jet) and having (porous media) rear stagnation points. Deposition efficiencies (deposition flux under unfavorable conditions normalized to deposition flux under favorable conditions) were consistently higher in the porous media relative to the impinging jet under the conditions compared (60), indicating that deposition was enhanced in systems having rear stagnation points. Similar recent comparisons of bacterial deposition in impinging jet versus porous media systems have demonstrated the same result (57, 61). These results are consistent with the possibility that, under unfavorable conditions, association of the microspheres with the porous media surfaces occurred via the secondary energy minimum and that these secondary-minimum-associated colloids were retained within stagnation zones in the porous media.

Potential mechanisms that would increase re-entrainment from secondary energy minima (e.g., rear stagnation points) and decrease deposition with increased flow rate include (i) decreased colloid retention capacity due to reduction of stagnation flow zone volumes, (ii) increased diffusion "out" of secondary minima (e.g., ref 56) driven by increased colloid concentration gradients away from zones of accumulation (e.g., rear stagnation points), (iii) increased magnitude of hydrodynamic collisions between mobile and surface-associated colloids, and (iv) increased dominance of hydrodynamic drag torques relative to adhesive torques created by protrusions. Distinction of these types of mechanisms will be greatly enhanced by direct observation of colloid deposition−re-entrainment dynamics.

In summary, hydrodynamic drag mitigates deposition and drives re-entrainment of near micrometer-sized colloids under unfavorable deposition conditions. This effect results in decreasing deposition rate coefficients and increasing re-entrainment rate coefficients, with increasing fluid velocity. Hydrodynamic drag is shown here to drive the readily observed and ubiquitous tailing of low concentrations of colloids during elution. The mechanisms by which increased hydrodynamic drag mitigates deposition and drives re-entrainment are likely closely linked to the processes that

govern the different forms of deviation of retained colloid profiles from log-linearity under unfavorable deposition conditions. Enhanced understanding of these mechanisms will enhance the development of models that accurately predict the magnitudes and trends of deposition rate coefficients, as well as the distributions of retained colloids in porous media under unfavorable conditions.

Acknowledgments

Literature Cited

(1) Yan, Y. D. Pulse-injection chromatographic determination of the deposition and release rate constants of colloidal particles in porous media. *Langmuir* **1996**, *12* (14), 3383−3388.

(2) Niehren, S.; Kinzelbach, W. Artificial colloid tracer tests: Development of a compact on-line microsphere counter and application to soil column experiments. *J. Contam. Hydrol.* **1998**, *35* (1−3), 249−259.

(3) Zhang, P.; Johnson, W. P. Low concentration microsphere transport in porous media. *Preprints of Extended Abstracts*, 217th ACS National Meeting, Anaheim, CA, **1999**, *39* (1), 281−283.

(4) Cumbie, D. H.; McKay, L. D. Influence of diameter on particle transport in a fractured shale saprolite. *J. Contam. Hydrol.* **1999**, *37* (1−2), 139−157.

(5) Grolimund, D. K.; Borkovec, M. Long-term release kinetics of colloidal particles from natural porous media. *Environ. Sci. Technol.* **1999**, *33* (2), 4054−4060.

(6) Fontes, D. E.; Mills, A. L.; Hornberger, G. M.; Herman, J. S. Physical and chemical factors influencing transport of microorganisms through porous media. *Appl. Environ. Microbiol.* **1991**, *57* (9), 2473−2481.

(7) Hornberger, G. M.; Mills, A. L.; Herman, J. S. Bacterial transport in porous media: Evaluation of a model using laboratory observation. *Water Resour. Res.* **1992**, *28* (3), 915−938.

(8) Lindqvist, R.; Cho, J. S.; Enfield, C. G. A kinetic model for cell density dependent bacterial transport in porous media. *Water Resour. Res.* **1994**, *30* (12), 3291−3299.

(9) McCaulou, D. R.; Bales, R. C.; McCarthy, J. F. Use of short-pulse experiments to study bacteria transport through porous media. *J. Contam. Hydrol.* **1994**, *15* (1−2), 1−14.

(10) McCaulou, D. R.; Bales, R. C.; Arnold, R. G. Effect of temperature-controlled motility on transport of bacteria and microspheres through saturated sediment. *Water Resour. Res.* **1995**, *31* (2), 271−280.

(11) Tan, Y.; Gannon, J. T.; Baveye, P.; Alexander, M. Transport of bacteria in an aquifer sand: Experiments and model simulations. *Water Resour. Res.* **1994**, *30* (12), 3243−3252.

(12) Johnson, W. P.; Blue, K. A.; Logan, B. E.; Arnold, R. G. Modeling bacteria detachment during transport through porous media as a residence-time-dependent process. *Water Resour. Res.* **1995**, *31* (11), 2649−2658.

(13) Harvey, R. W.; Kinner, N. E.; Bunn, A.; MacDonald, D.; Metge, D. W. Transport behavior of groundwater protozoa and protozoan-sized microspheres in sandy aquifer sediments. *Appl. Environ. Microbiol.* **1995**, *61* (1), 209−217.

(14) Harter, T.; Wagner, S.; Atwill, E. R. Colloid transport and filtration of cryptosporidium parvum in sandy soils and aquifer sediments. *Environ. Sci. Technol.* **2000**, *34* (1), 62−70.

(15) McCarthy, J. F. Colloid transport and mobilization in subsurface environments. *Preprints of Extended Abstracts*, 217th ACS National Meeting, Anaheim, CA, **1999**, *39* (1), 270−271.

(16) Harvey, R. W.; Garabedian, S. P. Use of colloid filtration theory in modeling movement of bacteria through a contaminated sandy aquifer. *Environ. Sci. Technol.* **1991**, *25* (1), 178−185.

(17) Zhang, P.; Johnson, W. P.; Scheibe, T. D.; Choi, K.; Dobbs, F. C.; Mailloux, B. J. Extended tailing of bacteria following breakthrough at the Narrow Channel Focus Area. *Water Resour. Res.* **2001**, *37* (11), 2687−2698.

(18) DeBorde, D. C.; Woessner, W. W.; Kiley, Q. T.; Ball, P. N. Rapid transport of viruses in a floodplain aquifer. *Water Res.* **1999**, *33* (10), 2229−2238.

(19) Redman, J. A.; Estes, M. K.; Grant, S. B. Resolving macroscale and microscale heterogeneity in pathogen filtration. *Colloids Surf. A* **2001**, *191* (1−2), 57−70.

(20) Davis, J. A. Adsorption of natural dissolved organic matter at the oxide/water interface. *Geochim. Cosmochim. Acta* **1982**, *46* (11), 2381−2393.

(21) Tipping, E.; Cooke, D. The effects of adsorbed humic substances on the surface charge of goethite (α-FeOOH) in freshwaters. *Geochim. Cosmochim. Acta* **1982**, *46* (1), 75−80.

(22) Shellenberger, K.; Logan, B. E. Effect of molecular scale roughness of glass beads on colloidal and bacterial deposition. *Environ. Sci. Technol.* **2002**, *36* (2), 184−189.

(23) Johnson, P. R.; Sun, N.; Elimelech, M. Colloid transport in geochemically heterogeneous porous media: Modeling and measurements. *Environ. Sci. Technol.* **1996**, *30* (11), 3284−3293.

(24) Hubbe, M. A. Theory of detachment of colloidal particles from flat surfaces exposed to flow. *Colloids Surf.* **1984**, *12*, 151−178.

(25) Hubbe, M. A. Detachment of colloidal hydrous oxide spheres from flat solids exposed to flow. *Colloids Surf.* **1985**, *16* (3), 249−270.

(26) Ryan, J. N.; Gschwend, P. M. Effects of ionic strength and flow rate on colloid release: Relating kinetics to intersurface potential energy. *J. Colloid Interface Sci.* **1994**, *164* (1), 21−34.

(27) Sharma, M. M.; Chamoun, H.; Sita Rama Sarma, D. S. H.; Schechter, R. S. Factors controlling the hydrodynamic detachment of particles from surfaces. *J. Colloid Interface Sci.* **1992**, *149* (1), 121−134.

(28) Bergendahl, J.; Grasso, D. Prediction of colloid detachment in a model porous media: Hydrodynamics. *Chem. Eng. Sci.* **2000**, *55* (9), 1523−1532.

(29) Varennes, S.; van de Ven, T. G. M. Deposition and detachment of latex particles at glass surfaces exposed to flow. *Phys. Chem. Hydrodynam.* **1987**, *9* (3−4), 537−559.

(30) Meinders, J. M.; Busscher, H. J. Influence of interparticle interactions on blocked areas and desorption during particle deposition to glass in a parallel plate flow chamber. *Langmuir* **1995**, *11* (1), 327−333.

(31) Compère, F.; Porel, G.; Delay, F. Transport and retention of clay particles in saturated porous media. Influence of ionic strength and pore velocity. *J. Contam. Hydrol.* **2001**, *49* (1−2), 1−21.

(32) Litton, G. M.; Olson, T. M. Colloid deposition rates on silica bed media and artifacts related to collector surface preparation methods. *Environ. Sci. Technol.* **1993**, *27* (1), 185−193.

(33) Li, X.; Scheibe, T. D.; Johnson, W. P. Apparent decreases in colloid deposition rate coefficient with distance of transport under unfavorable deposition conditions: A general phenomenon. *Environ. Sci. Technol.* **2004**, *38* (21), 5616−5625.

(34) Li, X.; Johnson, W. P. Nonmonotonic variations in deposition rate coefficients of microspheres in porous media under unfavorable deposition conditions. *Environ. Sci. Technol.* **2005**, *39* (6), 1658−1665.

(35) Scheibe, T. D.; Wood, B. D. A particle-based model of size or anion exclusion with application to microbial transport in porous media. *Water Resour. Res.* **2003**, *39* (4), doi 10.1029/2001WR001223.

(36) Rajagopalan, R.; Tien, C. Trajectory analysis of deep-bed filtration with the sphere-in-cell porous media model. *AIChE J.* **1976**, *22* (3), 523−533.

(37) Logan, B. E.; Jewett, D. G.; Arnold, R. G.; Bouwer, E. J.; O'Melia, C. R. Clarification of clean-bed filtration models. *J. Environ. Eng.* **1995**, *121* (12), 869−873.

(38) Tufenkji, N.; Elimelech, M. Correlation equation for predicting single-collector efficiency in physicochemical filtration in saturated porous media. *Environ. Sci. Technol.* **2004**, *38* (2), 529−536.

(39) Goldman, A. J.; Cox, R. G. Brenner, H. Slow viscous motion of a sphere parallel to a plane wall-II Couette flow. *Chem. Eng. Sci.* **1967**, *22* (4), 653−660.

(40) O'Neill, M. N. A sphere in contact with a plane wall in a slow linear shear flow. *Chem. Eng. Sci.* **1968**, *23* (11), 1293−1298.

(41) Ryan, J. N.; Elimelech, M. Colloid mobilization and transport in groundwater. *Colloids Surf. A* **1996**, *107*, 1−56.

(42) Tien, C. *Granular Filtration of Aerosols and Hydrosols*; Butterworth: Stoneham, MA, 1989.

(43) Lin, C. L.; Miller, J. D. Cone beam X-ray microtomography—A new facility for 3D analysis of multiphase materials. *Min. Metall. Process.* **2002**, *19* (2), 65−71.

(44) Lin, C. L.; Miller, J. D. Pore structure analysis of particle beds for fluid transport simulation during filtration. *Int. J. Min. Process.* **2004**, *73* (2−4), 281−294.

(45) Visser, J. *Surface and Colloid Science*; Matijević, E., Ed.; Wiley: New York, 1976.

(46) Bergendahl, J.; Grasso, D. Mechanistic basis for particle detachment from granular media. *Environ. Sci. Technol.* **2003**, *37* (10), 2317−2322.

(47) Visser, J. The adhesion of colloidal polystyrene particles to cellophane as a function of pH and ionic strength. *J. Colloid Interface Sci.* **1976**, *55* (3), 664−677.

(48) Israelachvili, J. N. *Intermolecular and Surface Forces*, 2nd ed.; Academic Press: London, 1992.

(49) Sader, J. E.; Chon, J. W. M.; Mulvaney, P. Calibration of rectangular atomic force microscope cantilevers. *Rev. Sci. Instrum.* **1999**, *70* (10), 3967−3969.

(50) Gregory, J., Interaction of unequal double layers at constant change. *J. Colloid Interface Sci.* **1975**, *51* (1), 44−51.

(51) Gregory, J., Approximate expressions for retarded van der Waals interaction. *J. Colloid Interface Sci.* **1981**, *83* (1), 138−145.

(52) Bergendahl, J.; Grasso, D. Prediction of colloidal detachment in a model porous media: Thermodynamics. *AIChE J.* **1999**, *45* (3), 475−484.

(53) Eichenlaub, S.; Gelb, A.; Beaudoin, S. Roughness models for particle adhesion. *J. Colloid Interface Sci.* **2004**, *280* (2), 289−298.

(54) Tufenkji, N.; Elimelech M. Deviation from classical colloid filtration theory in the presence of repulsive DLVO interactions. *Langmuir* **2004**, *20* (25), 10818−10828.

(55) Elimelech, M. Particle deposition on ideal collectors from dilute flowing suspensions: Mathematical formulation, numerical solution, and simulations. *Sep. Technol.* **1994**, *4* (4), 186−212.

(56) Hahn, M. W.; O'Melia, C. R. Deposition and reentrainment of Brownian particles in porous media under unfavorable chemical conditions: Some concepts and applications. *Environ. Sci. Technol.* **2004**, *38* (1), 210−220.

(57) Walker, S. L.; Redman, J. A.; Elimelech M. Role of Cell Surface Lipopolysaccharides (LPS) in *Escherichia coli* K12 Adhesion and Transport. *Langmuir* **2004**, *20* (18), 7736−7746.

(58) Prieve, D. C.; Lin, M. M. J. Adsorption of Brownian hydrosols onto a rotating disc aided by a uniform applied force. *J. Colloid Interface Sci.* **1979**, *76* (1), 32−47.

(59) Yang, C.; Dabros, T.; Li, D.; Czarnecki, J.; Masliyah, J. H., Kinetics of particle transport to a solid surface from an impinging jet under surface and external force fields. *J. Colloid Interface Sci.* **1998**, *208* (1), 226−240.

(60) Brow, C. N.; Li, X.; Rička, J.; Johnson, W. P. Comparison of microsphere deposition in porous media versus simple shear systems. *Colloids Surf. A* **2005**, *253* (1−3), 125−136.

(61) Redman, J. A.; Walker, S. L.; Elimelech, M. Bacterial adhesion and transport in porous media: Role of the secondary energy minimum. *Environ. Sci. Technol.* **2004**, *38* (6), 1777−1785.